International Journal of Heat and Fluid Flow 31 (2010) 208–216

Contents lists available at ScienceDirect

International Journal of Heat and Fluid Flow

journal homepage: www.elsevier.com/locate/ijhff

Suboptimal feedback control of flow over a sphere

Seung Jeon, Haecheon Choi *

School of Mechanical and Aerospace Engineering, Seoul National University, Seoul 151-744, Republic of Korea

ARTICLE INFO

Article history:
Received 17 July 2009
Received in revised form 5 December 2009
Accepted 17 December 2009
Available online 1 February 2010

Keywords:
Wake
Sphere
Suboptimal control
Drag reduction

ABSTRACT

In this study, we control unsteady motion in the wake behind a sphere using a suboptimal feedback control method based on the sensing of surface pressure. The cost function to be reduced is the square of the difference between the potential-flow and real pressures at the sphere surface. The actuation velocity (blowing/suction) is obtained from the suboptimal feedback control procedure. The sensing and actuation on the whole surface of the sphere is considered. This is an ideal case but provides a clear understanding of the effect of suboptimal feedback control on the present flow. We choose four different Reynolds numbers, Re = 100, 250, 300, and 425, covering four different flow regimes (steady axisymmetric, steady planar–symmetric, unsteady planar–symmetric, and unsteady asymmetric flows, respectively). With the present control, the vortex shedding disappears for Re = 300 and 425 and the drag is significantly reduced for all the Reynolds numbers considered.

1. Introduction

Flow over a bluff body is found in many engineering applications and vortex shedding behind a bluff body increases the mean drag and generates the drag and lift fluctuations. In particular the sphere is regarded as a representative three-dimensional bluff body, and its wake structure is quite complex because of three-dimensional vortex shedding (Achenbach, 1974b; Constantinescu and Squires, 2004; Johnson and Patel, 1999; Kim and Durbin, 1988; Mittal, 1999; Mittal and Najjar, 1999; Sakamoto and Haniu, 1990; Taneda, 1978; Yun et al., 2006). So far, many control methods have been developed for the purpose of mean drag and lift-fluctuation reduction. Those control methods may be classified as two groups: one by separation delay and the other by direct wake modification (Choi et al., 2008).

Examples of drag reduction by separation delay include slip wall (Choi and Choi, 2000; Milano and Koumoutsakos, 2002; Poncet and Koumoutsakos, 2005), optimal and suboptimal blowing and suction (Ghattas and Bark, 1997; He et al., 2000; Homescu et al., 2002; Li et al., 2003; Milano and Koumoutsakos, 2002; Min and Choi, 1999; Protas and Styczek, 2002), time-periodic blowing and suction (Fujisawa et al., 2004; Jeon et al., 2004; Lin et al., 1995; Williams et al., 1992), and surface modifications such as dimple (Bearman and Harvey, 1976; Choi et al., 2006), roughness (Achenbach, 1974a; Shih et al., 1994) and seam (Higuchi, 2005). With these control methods, the streamwise velocity profile inside the boundary layer becomes fuller and separation is delayed, resulting in drag reduction.

Drag reduction has also been achieved by direct wake modification. That is, with active or passive control, vortex shedding behind a bluff body is weakened through the change in its structure and drag is reduced. In this case, the drag reduction is not necessarily accompanied by the delay of separation. Examples include the splitter plate (Anderson and Szewczyk, 1997; Hwang et al., 2003; Kwon and Choi, 1996; Ozono, 1999), base bleed (Bearman, 1967; Wood, 1964), uniform blowing (Bagchi, 2007), actuation based on the sensing of flow variable in the wake (Berger, 1967; Bergmann et al., 2005; Cortelezzi, 1996; Cortelezzi et al., 1997; Ffowcs and Zhao, 1989; Gillies, 1998; Graham et al., 1999; Huang, 1996; Li and Aubry, 2003; Park et al., 1994; Protas, 2004; Roussopoulos, 1993), ventilation (Suryanarayana and Meier, 1995), and geometry modification (Bearman and Owen, 1998; Darekar and Sherwin, 2001; Owen et al., 2000, 2001; Park et al., 2006; Petrusma and Gai, 1994; Rodriguez, 1991; Tanner, 1972; Tombazis and Bearman, 1997; Zdravkovich, 1981), blowing and suction (Kim and Choi, 2005; Kim et al., 2004) and wall slip (Poncet et al., 2008) varying along the spanwise direction.

A summary about most of studies mentioned above was given by Choi et al. (2008), and thus we do not repeat it here. In the present study, our objective is to reduce drag on a sphere using an active feedback control. Thus, in the below, we discuss results from previous active controls applied to a sphere. In addition, the results from active controls of three-dimensional flow over a circular cylinder are discussed here, because the response of this flow to actuations may have common features with that of flow over a sphere (see, for example, Mittal and Najjar, 1999).

* Corresponding author. Tel.: +82 2 880 8361; fax: +82 2 878 3662.
E-mail address: choi@snu.ac.kr (H. Choi).

0142-727X/$ - see front matter © 2009 Elsevier Inc. All rights reserved.
doi:10.1016/j.ijheatfluidflow.2009.12.010

Ghattas and Bark (1997) applied an optimal control to the flow over a sphere to minimize a cost function (rate of energy dissipation). They provided blowing and suction based on the sensing of whole velocity field and the cost function was reduced. As a result, the recirculation region disappeared. However, they considered only a steady state base flow at Re = 130.

Milano and Koumoutsakos (2002) and Poncet and Koumoutsakos (2005) controlled two- and three-dimensional flows over a circular cylinder using wall slip or blowing/suction at $\mathrm{Re} = u_\infty d_c/\nu = 500$, where u_∞ is the free-stream velocity, d_c the cylinder diameter, and ν the kinematic viscosity. The optimal distribution of each actuation was obtained from a clustering genetic algorithm. The mechanism of drag reduction was the separation delay. Based on the comparison of results from two types of actuations, they concluded that the wall slip has a wider parameter space for drag reduction than the blowing and suction. It was also shown that the amount of drag reduction is proportional to the square of control input energy and the force oscillations are inversely proportional to the control input energy.

Jeon et al. (2004) conducted an active control of the flow over a sphere at $\mathrm{Re} = 6 \times 10^4 \sim 2 \times 10^5$ by providing a high-frequency blowing/suction from a slot located just before the separation point. The disturbances from the high-frequency forcing grew inside the boundary layer, which delayed laminar separation and reattached separated flow through the growth of the disturbances along the separating shear layer. Consequently, main separation was delayed and a significant amount of drag reduction was achieved.

Kim and Choi (2005) applied a distributed forcing to flow over a circular cylinder: a sinusoidal blowing and suction in the spanwise direction (but constant in time) from the slots located at upper and lower surfaces of the cylinder. Both laminar and turbulent flows in the wake were considered. It was shown that the forcing attenuates or annihilates the vortex shedding through the phase mismatch along the spanwise direction in the vortex shedding process and thus significantly reduces the mean drag and the drag and lift fluctuations.

Niazmand and Renksizbulut (2005) investigated the effect of non-uniform blowing (maximum at the stagnation point and 0 at the base point, respectively) on the flow over a spinning sphere at 10 < Re < 300. With the blowing, the drag was reduced from the reduction in the skin friction at low Re's (Re = 200 and 250), but the amount of drag reduction was negligible at Re = 300. Bagchi (2007) investigated the effect of uniform blowing or suction on the flow over a sphere at $1 \leqslant \mathrm{Re} \leqslant 300$. Owing to the blowing, the onset of recirculation was delayed to a higher Reynolds number ($\mathrm{Re} \geqslant 38$), but the length of recirculation was enlarged. The drag was reduced from the decrease in the skin friction, but the amount of drag reduction decreased with increasing Reynolds number. On the other hand, the suction eliminated the recirculation region in the wake but increased drag due to the increase in the skin friction.

Poncet et al. (2008) controlled the flow past a circular cylinder at Re = 300 by the wall slip varying in the spanwise direction. The optimal wall slip distribution was obtained from parameter optimization and resulted in a higher drag reduction than that from uniform wall slip along the spanwise direction. They showed that the streamwise vortex braids introduced by the spatially varying wall slip weaken the primary spanwise vortices in the wake and the drag is reduced. This mechanism is similar to that of Kim and Choi (2005).

The vortical structure in the sphere wake is three-dimensional and there is no primary azimuthal vortex in this flow unlike the case of cylinder wake. Therefore, an introduction of spanwise modulation into the flow over a sphere may add more three-dimensionality to the wake and may not reduce the mean drag and lift fluctuations (Choi et al., 2008). This is very different from the case of flow over a circular cylinder, in which three-dimensional modulation breaks the two-dimensional primary vortex into three-dimensional one, reducing its strength and drag (Darekar and Sherwin, 2001; Kim and Choi, 2005; Poncet et al., 2008; Tombazis and Bearman, 1997). Therefore, it is important to develop a control method for the flow over a sphere for the reduction of mean drag and lift fluctuations.

Significant efforts have been made in developing systematic control methods based on the mathematical theory such as the optimal, suboptimal, and linear controls (see for reviews Bewley, 2001; Choi et al., 2008; Collis et al., 2004; Kim and Bewley, 2007). In the present study, we apply the suboptimal control to flow over a sphere for drag reduction. The suboptimal control algorithm was first suggested by Choi et al. (1993) and further applied to various flows (Lee et al., 1998; Min and Choi, 1999; Kang and Choi, 2002). The objective of present study is to see the performance of this control in manipulating three-dimensional vortical structures in the wake behind the sphere. The suboptimal control procedure is briefly introduced in Section 2, and the numerical method is given in Section 3. The control results are shown and discussed in Section 4, followed by a summary in Section 5.

2. Suboptimal control method

2.1. Cost function

The choice of cost function to be reduced is one of the most important steps in the optimal and suboptimal controls. In the present study, we choose the cost function as

$$J(\psi) = \int_{\Gamma_s} (p_t - p(\theta,\phi))^2 R^2 \sin\theta d\theta d\phi, \tag{1}$$

where ψ is the actuation (blowing/suction) on the control region (Γ_c), Γ_s the sensing region, p_t the target pressure, R the sphere radius, $p(\theta,\phi)$ the pressure on Γ_s, and θ and ϕ denote the polar and azimuthal angles, respectively (Fig. 1). The sensing (Γ_s) and control (Γ_c) regions are the sphere surface. The cost function Eq. (1) is the square of the difference between the target and real pressures on the sphere surface. In this study, the target pressure is set to be that of potential flow, aiming that the controlled flow has a large pressure recovery on the rear surface of the sphere. We also tested another cost function (form drag), $J(\psi) = \int_{\Gamma_s} (p(\theta,\phi)\cos\theta) R^2 \sin\theta d\theta d\phi$, but the control result was much better with Eq. (1) in terms of reducing the mean drag and lift fluctuations. This result is similar to that shown for the case of circular cylinder (Min and Choi, 1999).

2.2. Suboptimal control procedure

At each instant of time, an actuation ψ of reducing J is found iteratively. That is, $J(\psi^{k+1}(t)) < J(\psi^k(t))$, where k is the iteration index. From the Taylor series expansion,

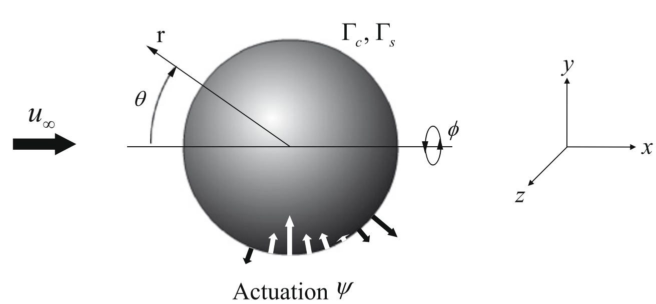

Fig. 1. Schematic diagram of the coordinates and suboptimal feedback control.

$$J\left(\psi^{k+1}(t)\right) \approx J\left(\psi^{k}(t)\right) + \frac{\mathscr{D}J\left(\psi^{k}(t)\right)}{\mathscr{D}\psi}\left(\psi^{k+1}(t) - \psi^{k}(t)\right), \tag{2}$$

where

$$\frac{\mathscr{D}J}{\mathscr{D}\psi}\tilde{\psi} = \lim_{\epsilon\to 0}\frac{J(\psi+\epsilon\tilde{\psi}) - J(\psi)}{\epsilon} \tag{3}$$

and $\tilde{\psi}$ is an arbitrary perturbation to ψ. To satisfy $J(\psi^{k+1}(t)) < J(\psi^{k}(t))$ from Eq. (2), a gradient algorithm is used,

$$\psi^{k+1}(t) - \psi^{k}(t) = -\alpha\frac{\mathscr{D}J\left(\psi^{k}(t)\right)}{\mathscr{D}\psi}, \tag{4}$$

where $\alpha(>0)$ is the descent parameter. One may obtain the optimal actuation, ψ, from the iteration of Eq. (4). However, this iteration process is computationally possible but impossible in real experiment because the flow variable should be measured iteratively. It is also known from Choi et al. (1993) that the cost function is significantly reduced at the first iteration. Therefore, for the practical implementation within the framework of suboptimal control, we do not perform any iteration. In other words, we do not pursue global optimization for practical implementation. Then, the actuation of reducing J is found at each control time as follows:

$$\psi(t) = -\alpha\frac{\mathscr{D}J}{\mathscr{D}\psi}. \tag{5}$$

Here, the parameter α is chosen to lead to a given maximum value of ψ, which provides a regularity in the system answer, and $\mathscr{D}J/\mathscr{D}\psi$ is obtained from Eq. (1)

$$\frac{\mathscr{D}J}{\mathscr{D}\psi}\tilde{\psi} = \int_{\Gamma_s} -2(p_t - p(\theta,\phi))\frac{\mathscr{D}p}{\mathscr{D}\psi}\tilde{\psi}R^2\sin\theta d\theta d\phi. \tag{6}$$

We use the Navier–Stokes and continuity equations to evaluate $\mathscr{D}p/\mathscr{D}\psi$ in Eq. (6) and the procedure is explained in the below.

The governing equations of fluid flow are the incompressible Navier–Stokes and continuity equations, non-dimensionalized by the free-stream velocity u_∞ and the sphere diameter d,

$$\frac{\partial u_i}{\partial t} + \frac{\partial u_i u_j}{\partial x_j} = -\frac{\partial p}{\partial x_i} + \frac{1}{\mathrm{Re}}\frac{\partial^2 u_i}{\partial x_j \partial x_j}, \tag{7}$$

$$\frac{\partial u_i}{\partial x_i} = 0, \tag{8}$$

with the boundary conditions

$$\begin{cases} \mathbf{u} = \psi(\theta,\phi)\hat{r} & \text{on } \Gamma_c \\ \mathbf{u} = \text{given (in Section3)} & \text{elsewhere} \end{cases}, \tag{9}$$

where t is time, x_i the coordinates, $u_i(=\mathbf{u})$ the corresponding velocity components, p the pressure, and $\hat{r}$ is the unit vector in the radial direction. Eqs. (7)–(9) are discretized in time using an implicit method (e.g. Crank–Nicolson method) for the linear terms and an explicit method (e.g. a third-order Runge–Kutta method) for the nonlinear terms (see on how to choose these discretization methods Choi et al., 1993; Min and Choi, 1999:

$$u_i^{n+1} + \frac{\Delta t_c}{2}\frac{\partial p^{n+1}}{\partial x_i} - \frac{\Delta t_c}{2\mathrm{Re}}\frac{\partial^2 u_i^{n+1}}{\partial x_j \partial x_j} = RHS_i^n, \tag{10}$$

$$\frac{\partial u_i^{n+1}}{\partial x_i} = 0, \tag{11}$$

and

$$\begin{cases} \mathbf{u}^{n+1} = \psi^{n+1}(\theta,\phi)\hat{r} & \text{on } \Gamma_c \\ \mathbf{u}^{n+1} = \text{given} & \text{elsewhere} \end{cases}, \tag{12}$$

where Δt_c is the control time interval, the superscript $n+1$ denotes the next control time step at which a new actuation is applied, and RHS_i^n includes all the terms associated with the control time step n. We define q_i and ρ using the Fréchet differential as follows:

$$q_i = \frac{\mathscr{D}u_i^{n+1}}{\mathscr{D}\psi^{n+1}}\tilde{\psi}^{n+1}, \tag{13}$$

$$\rho = \frac{\mathscr{D}p^{n+1}}{\mathscr{D}\psi^{n+1}}\tilde{\psi}^{n+1}. \tag{14}$$

Taking the Fréchet differential to Eqs. (10)–(12), we obtain the following:

$$q_i + \frac{\Delta t_c}{2}\frac{\partial \rho}{\partial x_i} - \frac{\Delta t_c}{2\mathrm{Re}}\frac{\partial^2 q_i}{\partial x_j \partial x_j} = 0, \tag{15}$$

$$\frac{\partial q_i}{\partial x_i} = 0, \tag{16}$$

and

$$\begin{cases} \mathbf{q} = \tilde{\psi}(\theta,\phi)\hat{r} & \text{on } \Gamma_c \\ \mathbf{q} = 0 & \text{elsewhere} \end{cases} \tag{17}$$

The q_i and ρ are obtained from the following convolution integral:

$$\begin{aligned} q_i(r,\theta,\phi) &= \int_{\Gamma_c}\eta_i(r,\theta-\theta',\phi-\phi')\tilde{\psi}(\theta',\phi')r^2\sin\theta' d\theta' d\phi', \\ \rho(r,\theta,\phi) &= \int_{\Gamma_c}\Pi(r,\theta-\theta',\phi-\phi')\tilde{\psi}(\theta',\phi')r^2\sin\theta' d\theta' d\phi'. \end{aligned} \tag{18}$$

Here η_i and Π are the solutions of the following equations and boundary conditions:

$$\eta_i + \frac{\Delta t_c}{2}\frac{\partial \Pi}{\partial x_i} - \frac{\Delta t_c}{2\mathrm{Re}}\frac{\partial^2 \eta_i}{\partial x_j \partial x_j} = 0, \tag{19}$$

$$\frac{\partial \eta_i}{\partial x_i} = 0, \tag{20}$$

and

$$\begin{cases} \boldsymbol{\eta} = \delta(\theta,\phi)\hat{r} & \text{on } \Gamma_c \\ \boldsymbol{\eta} = 0 & \text{elsewhere} \end{cases}, \tag{21}$$

where δ is the Dirac delta function.

Once Π is obtained, Eq. (6) becomes

$$\begin{aligned} \frac{\mathscr{D}J(\theta,\phi)}{\mathscr{D}\psi} = \int_{\Gamma_s} & -2(p_t - p(\theta',\phi'))\Pi(\theta'-\theta,\phi'-\phi)R^2 \\ & \times \sin\theta' d\theta' d\phi', \end{aligned} \tag{22}$$

where θ' and ϕ' are the polar and azimuthal angles used for the convolution integral, respectively. Then, from Eq. (5), the actuation ψ becomes

$$\psi^{n+1}(\theta,\phi) = 2\alpha\int_{\Gamma_s}(p_t - p(\theta',\phi'))\Pi(\theta'-\theta,\phi'-\phi)R^2\sin\theta' d\theta' d\phi'. \tag{23}$$

As shown in Eq. (23), the pressure on Γ_s is measured at each control time. However, Π is evaluated only one time before the start of control, because the governing equations for Π, Eqs. (19)–(21), do not contain any time-varying variables. The value of α is chosen such that the maximum value of ψ is $\psi_{max} = 0.05u_\infty$, $0.1u_\infty$ or $0.15u_\infty$. For example, for $\psi_{max} = 0.1u_\infty$, α varies in time and ranges from 335 to 460 (Re = 425). To enforce the zero-net mass flow rate from control, the mean value of ψ is subtracted from ψ.

In our computations, the sensors and actuators occupy the same positions on the sphere surface, which cannot be realized in a practical setting. To realize the present control into practical situations, one may place the sensors and actuators alternately along the streamwise direction (and the azimuthal direction), and obtain the actuation distribution at Γ_c from Eq. (23) with the sensing pressure at Γ_s.

3. Numerical method

We use an immersed boundary method (IB method) in a cylindrical coordinate to solve Eqs. (7)–(9). Using an IB method (Kim et al., 2001), we obtained accurate solutions for flow over a sphere at low and high Reynolds numbers (Kim et al., 2001; Kim and Choi, 2002; Yun et al., 2006). In the present case containing time-varying blowing and suction, however, artificial oscillations are observed in the pressure near the immersed boundary and in the time history of drag on the sphere. Therefore, we devise a modified version of IB method to remove or significantly attenuate the artificial oscillations, and briefly explain it here.

The governing equations and boundary conditions with an IB method are

$$\frac{\partial u_i}{\partial t}+\frac{\partial u_i u_j}{\partial x_j}=-\frac{\partial p}{\partial x_i}+\frac{1}{\mathrm{Re}}\frac{\partial^2 u_i}{\partial x_j \partial x_j}+f_i, \tag{24}$$

$$\frac{\partial u_i}{\partial x_i}-q=0, \tag{25}$$

and

$$\mathbf{u}=\psi(\theta,\phi,t)\hat{r} \text{ on } \Gamma_c, \tag{26}$$

where f_i and q are the momentum forcing and mass source/sink, respectively. A staggered grid system is used such that u_i and f_i are defined at the cell surface, and p and q are defined at the cell center. The detailed procedures of obtaining f_i and q are found in Kim et al. (2001).

To solve Eqs. (24)–(26), a fractional step method is used (see Kim and Choi, 2002 for the detail). In the second step of the fractional step method, one has to solve a Poisson equation for the pseudo-pressure together with the Neumann boundary condition. In Kim et al. (2001), the Neumann boundary condition is applied only at the outer boundary as shown in Fig. 2a. In the present IB method, the Neumann boundary condition is also applied at the immersed boundary. This modification removes or significantly reduces the force oscillations (Jeon and Choi, 2009).

The computational domain size in the cylindrical coordinate is $-15d \leqslant x \leqslant 15d$, $0 \leqslant r \leqslant 15d$, and $0 \leqslant \theta < 2\Pi$, Dirichlet boundary conditions ($u_x = u_\infty$, $u_r = u_\theta = 0$) are applied at the inflow and far-field boundaries and a convective boundary condition ($\partial u_i/\partial t + c\partial u_i/\partial x = 0$) is used for the outflow boundary, where c is the plane-averaged streamwise velocity at the exit.

We consider four different Reynolds numbers, Re = 100, 250, 300, and 425, representing four different flow regimes, steady axisymmetric, steady planar–symmetric, unsteady planar–symmetric, and unsteady asymmetric flows, respectively. The numbers of grid points used are, $145(x) \times 61(r) \times 65(\theta)$, $193(x) \times 91(r) \times 65(\theta)$, $289(x) \times 161(r) \times 65(\theta)$ and $449(x) \times 161(r) \times 65(\theta)$, respectively, for Re = 100, 250, 300, and 425. The computational time step is $\Delta t = 0.01d/u_\infty$. The numerical accuracy was confirmed by increasing the number of grid points in each direction. Fig. 3 shows the instantaneous vortical structures identified using the method of Jeong and Hussain (1995). As shown, four different flow regimes are well identified from this figure. This result agrees very well with those obtained by Johnson and Patel (1999), Kim et al. (2001) and Kim and Choi (2002).

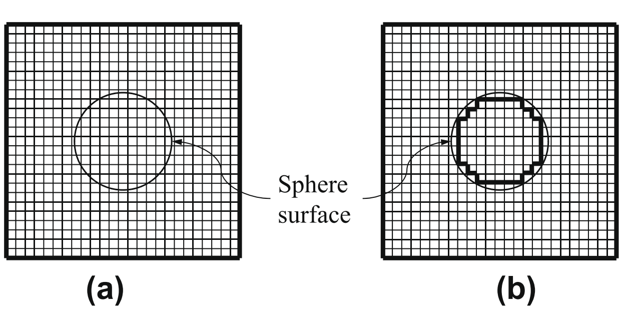

Fig. 2. Boundary condition for pseudo-pressure: (a) original IB method and (b) modified IB method. The thick solid lines denote the grid lines where the Neumann boundary condition for pseudo-pressure is satisfied.

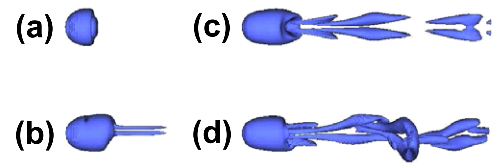

Fig. 3. Instantaneous vortical structures: (a) Re = 100 (steady axisymmetric); (b) 250 (steady planar–symmetric); (c) 300 (unsteady planar–symmetric); and (d) 425 (unsteady asymmetric).

The control time interval of updating the actuation based on Eq. (23) is set to be $\Delta t_c = 0.05d/u_\infty$. The control result is not much affected by the choice of Δt_c, once Δt_c is much smaller than the period of vortex shedding. For example, for each Reynolds number, the final flow state from the control with $\Delta t_c = 0.5d/u_\infty$ is nearly the same as that with $\Delta t_c = 0.05d/u_\infty$. On the other hand, when Δt_c is very small such as $\Delta t_c = \Delta t$ (meaning that the actuation is updated at every computational time step), the surface pressure reacts on the actuation itself rather than on the flow change due to the actuation. That is, in this case, the sensor and actuator talk to each other regardless of the flow modification by the actuation. Therefore, it is required to have $\Delta t_c > \Delta t$ to avoid this problem: practically, Δt_c larger than $3 \sim 4\Delta t$ is good enough.

4. Results

Fig. 4a shows the instantaneous surface pressure coefficients ($C_P = (p - p_\infty)/\frac{1}{2}\rho u_\infty^2$) along the polar angle (θ) at several azimuthal angles (ϕ) for Re = 425 (see Fig. 3d for uncontrolled flow), together with the surface pressure of potential flow. Although the vortical structure in the wake is fully three-dimensional, the variation of C_P along the azimuthal angle is weak. Thus, the actuation velocity slightly varies along the azimuthal angle (Fig. 4b). On the other hand, ψ significantly varies along the polar angle like the variation of C_P. The ψ is negative near $\theta = 90°$ and positive near the stagnation and base points, meaning that suction is applied near $\theta = 90°$ and blowing near $\theta = 0°$ and 180°. Because of the suction around $\theta = 90°$, the near-wall velocity profile becomes fuller and the separation delays, resulting in the recovery of the pressure on the rear surface (Fig. 5). As shown in Fig. 5, with larger ψ_{max}, the near-wall velocity profile becomes fuller and C_P recovers more on the rear surface. Therefore, the skin friction increases and the form drag significantly decreases with the present suboptimal control. Fig. 6 shows the variations of cost function, and total drag, lift and skin-friction drag coefficients for Re = 425:

$$\begin{aligned}
C_D &= (total\ drag)/\tfrac{1}{2}\rho u_\infty^2 \pi R^2,\\
C_L(magnitude\ of\ lift\ coefficient) &= \sqrt{C_y^2+C_z^2},\\
C_f &= (friction\ drag)/\tfrac{1}{2}\rho u_\infty^2 \pi R^2.
\end{aligned} \tag{27}$$

Here, C_y and C_z are the lift coefficients in y and z directions, respectively. As expected, the cost function decreases further with increasing ψ_{max}. The total drag and lift coefficients also decrease with the control, whereas the skin-friction drag increases as we expect from Fig. 5a.

The performance of the present suboptimal control is summarized in Table 1. Note that the present drag coefficients of uncontrolled flow agree well with those of Johnson and Patel (1999)

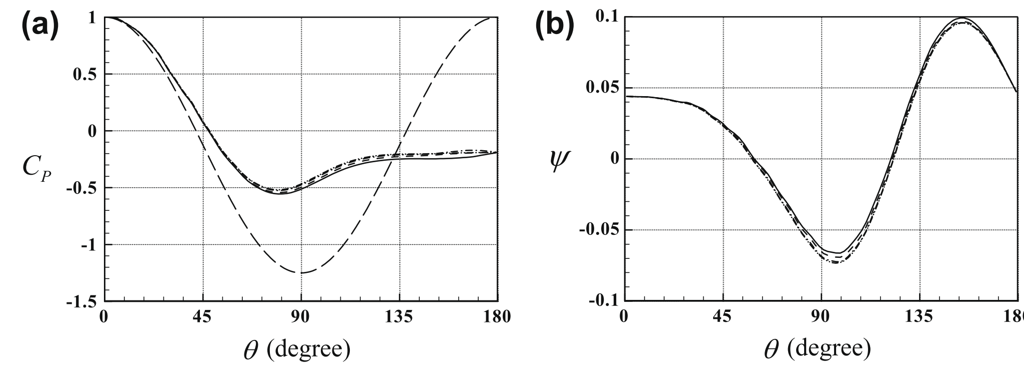

Fig. 4. Instantaneous surface pressure coefficients and actuation velocities along the polar angle at several azimuthal angles for Re = 425 ($tu_\infty/d = 0$; just before control): (a) C_P and (b) $\psi(\psi_{max} = 0.1u_\infty)$. —, $\phi = 56°$; –·–, 146°; – – –, 236°; –··–, 326°. The long dashed line in (a) denotes the surface pressure of potential-flow.

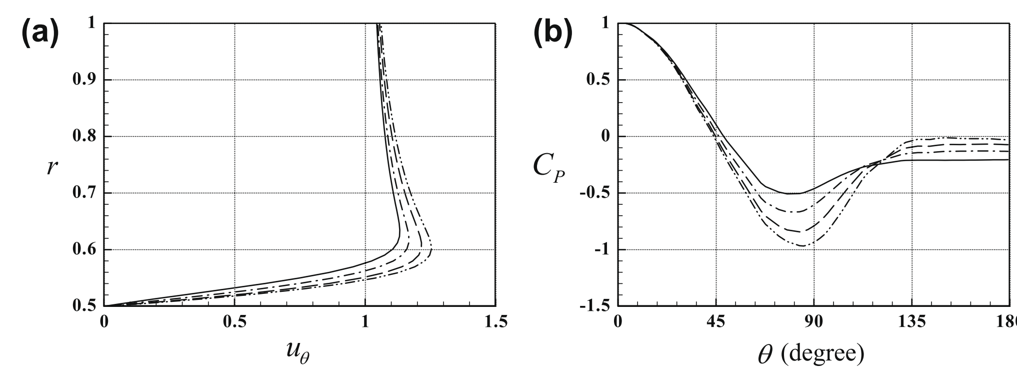

Fig. 5. Profiles of the polar velocity and surface pressure coefficient (Re = 425): (a) u_θ at $\theta = 90°$; (b) C_P. —, No control; –·–, $\psi_{max}/u_\infty = 0.05$; – – –, 0.1; –··–, 0.15.

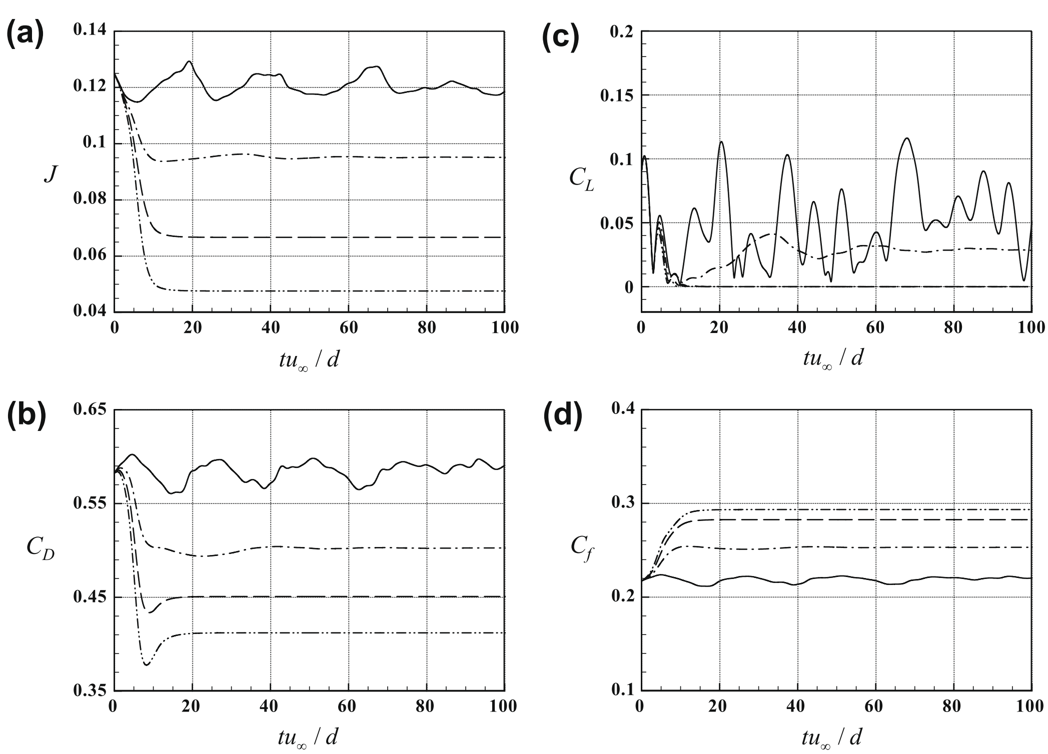

Fig. 6. Time histories of the cost function, and total drag, lift and skin-friction drag coefficients (Re = 425): (a) J; (b) C_D; (c) C_L; and (d) C_f. —, No control; –·–, $\psi_{max}/u_\infty = 0.05$; – – –, 0.1; –··–, 0.15.

Table 1
Performance of the control. C_{D_0} and C_{L_0} are the total drag and lift coefficients in the case of no control. See Eq. (27) for the definitions of C_D and C_L, and Eqs. (28) and (29) for the definitions of γ_i and γ_a, respectively. S, P, and A denote the axisymmetric, planar–symmetric, asymmetric flows, respectively.

Re	C_{D_0}	C_{L_0}	ψ_{max}/u_∞	$\frac{(C_D-C_{D_0})}{C_{D_0}}$ (%)	$\frac{(C_L-C_{L_0})}{C_{L_0}}$ (%)	Efficiency		Flow characteristics after control
						γ_i	γ_a	
100	1.087	0	0.05	−2.2	–	1.100	0.696	Steady S
(Steady S)			0.10	−4.8	–	1.099	0.768	Steady S
			0.15	−7.7	–	1.098	0.824	Steady S
250	0.702	0.060	0.05	−6.6	−100	2.015	1.415	Steady S
(Steady P)			0.10	−12.0	−100	1.715	1.301	Steady S
			0.15	−17.4	−100	1.648	1.306	Steady S
300	0.657	0.067	0.05	−9.5	−86.8	2.754	1.948	Steady P
(Unsteady P)			0.10	−16.1	−100	2.091	1.578	Steady S
			0.15	−21.4	−100	1.915	1.516	Steady S
425	0.587	0.061	0.05	−14.4	−53.4	3.870	2.675	Unsteady P
(Unsteady A)			0.10	−23.2	−100	2.858	2.128	Steady S
			0.15	−29.8	−100	2.496	1.945	Steady S

where $C_{D_0} = 0.70$ and $C_{L_0} = 0.062$ for Re = 250, and $C_{D_0} = 0.656$ and $C_{L_0} = 0.069$ for Re = 300, respectively. The control efficiency is defined as the ratio of the save power to the control input power. As indicated by Choi et al. (2008), a rigorous estimation of the efficiency is not easy because it depends on how the mechanism of the control device is set up to realize the control input in practical situations. The ideal control efficiency may be defined as (Choi et al., 2008)

$$\gamma_i = \frac{\pi R^2 (C_{D_0} - C_D)}{\int_{\Gamma_c} (\psi^3 + 2p\psi + \frac{4}{\mathrm{Re}}\frac{2}{R}\psi^2) R^2 \sin\theta d\theta d\phi}. \tag{28}$$

The first term in the control input power is the energy convection, the second one is the pressure work, and the third one is from the surface curvature (Fukagata et al., 2009). On the other hand, the lowest possible control efficiency may be defined as

$$\gamma_a = \frac{\pi R^2 (C_{D_0} - C_D)}{\int_{\Gamma_c} (|\psi^3| + 2|p\psi| + \frac{4}{\mathrm{Re}}\frac{2}{R}\psi^2) R^2 \sin\theta d\theta d\phi}. \tag{29}$$

The actual efficiency of a control method may be in between γ_i and γ_a. See Choi et al. (2008) for more discussion on the control efficiency. The efficiencies γ_i and γ_a for all the control cases except at Re = 100 are higher than 1, indicating that the present suboptimal control is cost effective. The efficiency γ_a increases with increasing Reynolds number, but (with the exception of Re = 100) decreases with increasing ψ_{max}, although the percentage of drag reduction increases further with increasing ψ_{max}. When we look at the control power input, the values of $\int_{\Gamma_c} |\psi^3| R^2 \sin\theta d\theta d\phi$ and $\int_{\Gamma_c} \frac{4}{\mathrm{Re}}\frac{2}{R}\psi^2 R^2 \sin\theta d\theta d\phi$ are much smaller than that of $\int_{\Gamma_c} 2|p\psi| R^2 \sin\theta d\theta d\phi$. That is, the pressure work consumes most of control power input.

The values of C_L decrease for all the control cases. At large ψ_{max}'s (0.1 and $0.15u_\infty$), the flow becomes steady and C_L becomes zero. Fig. 7 shows the instantaneous vortical structures in the wake at Re = 425 for different ψ_{max}'s. As shown, at ψ_{max} = 0.1 and $0.15u_\infty$, the flow becomes steady axisymmetric, but is unsteady planar–symmetric at $\psi_{max} = 0.05u_\infty$. The isolated vortices observed in the wake in Fig. 7b and c represent the recirculating flows shifted downstream due to the control. A similar phenomenon was also found for flow over a sphere with uniform blowing by Bagchi (2007). The vortical structures at other Reynolds numbers look similar to those in Fig. 7b and c when the controlled flows become steady. The change in the flow characteristics due to control is described in Table 1.

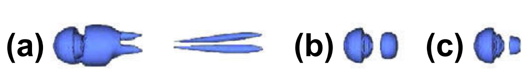

Fig. 7. Instantaneous vortical structures at Re = 425: (a) ψ_{max}/u_∞ = 0.05; (b) 0.1; and (c) 0.15.

The actuation profile from the suboptimal control for Re = 425 is given as a dashed line in Fig. 8, showing suction near θ = 90° and blowing near θ = 0° and 180°. It is expected that the suction near θ = 90° and blowing near 180° provide drag reduction, respectively, because the suction delays the separation and the blowing near the base point provides a thrust to the body as well as reduces the interaction of vortices growing along the separating shear layer. On the other hand, it was shown from Bagchi (2007) that, at low Reynolds number, uniform blowing reduces the drag through the decrease in the skin friction but uniform suction increases the drag even with elimination of recirculation region. Therefore, we apply the suction and blowing profiles obtained from the present approach separately to flow over a sphere, to see how each of these actuation profiles plays a role of drag reduction. Fig. 8a and b shows the corresponding blowing and suction profiles (called blowing and suction controls, respectively, hereafter). Fig. 9 shows the results of blowing and suction controls for Re = 425, together with those of no control and suboptimal feedback control. The surface pressure is recovered much more by suction control than by blowing control, and the overall shape of C_p from suction control is nearly same as that from suboptimal control (Fig. 9a). Thus, the amount of form drag reduction is much more with suction control than with blowing control (Fig. 9b). The friction drag is significantly increased by suction control, whereas it is decreased by blowing control (Fig. 9c). This result is similar to that shown in Bagchi (2007). The friction drag from suboptimal control is increased but the amount of increase is smaller than that of suction control due to the contribution from blowing control. It is interesting to see that the total drag is reduced more by blowing control than suction control although the pressure recovery is large from suction control. Therefore, the blowing part in the suboptimal actuation profile plays an important role in reducing drag. The instantaneous vortical structures from blowing and suction controls, shown in Fig. 10, are similar to those of no control and suboptimal control, respectively. This result is also expected from the distributions of surface pressure coefficient shown in Fig. 9a. However, there is a difference between the suction and suboptimal controls, in that the flow structure in the wake is steady planar–symmetric for suction control but is steady axisymmetric for suboptimal control. Therefore, the combined effect from both suction and blowing controls is necessary to obtain the present results of suboptimal control.

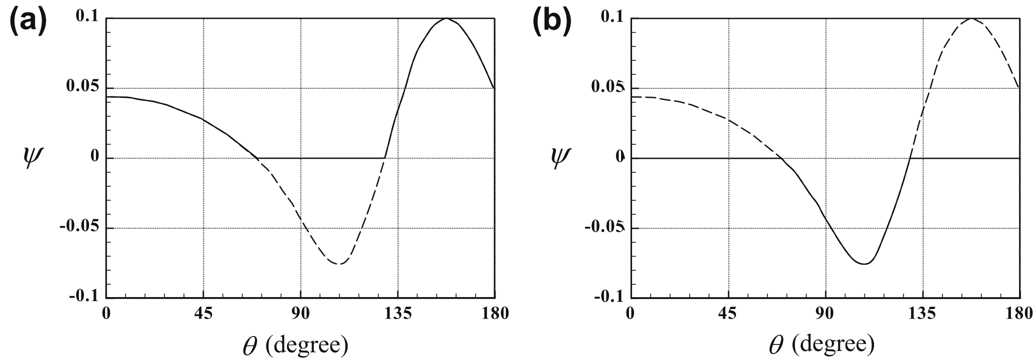

Fig. 8. Open-loop actuation profiles along the polar angle (Re = 425 and $\psi_{max} = 0.1u_\infty$): (a) blowing control and (b) suction control. The dashed line is the suboptimal actuation profile.

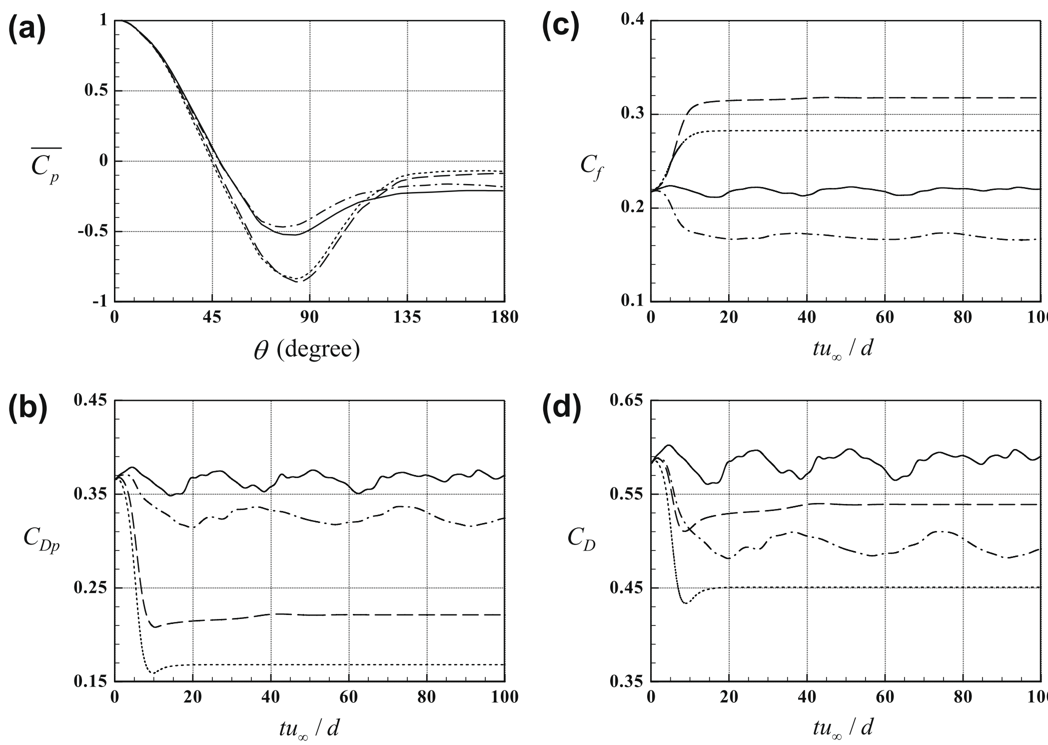

Fig. 9. Control results from blowing and suction controls (Re = 425 and $\psi_{max} = 0.1u_\infty$): (a) surface pressure coefficient; (b) form drag; (c) friction drag; and (d) total drag. —, No control; –·–, blowing control; – – –, suction control; · · · · · ·, suboptimal control.

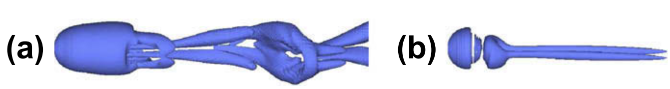

Fig. 10. Instantaneous vortical structures at Re = 425 and $\psi_{max} = 0.1u_\infty$: (a) blowing control and (b) suction control.

5. Summary

In the present study, we developed a suboptimal feedback control method for flow over a sphere. The cost function to be reduced was the square of the difference in the surface pressure between the real and potential flows. The actuation (blowing/suction) velocity on the sphere surface was determined based on the sensing of surface pressure through the suboptimal control procedure. Using this suboptimal control, the suction was applied near the top and bottom surfaces of the sphere and the blowing was given near the stagnation and base points. Due to the suction part, the polar velocity became fuller near the surface and delayed separation, resulting in the pressure recovery at the rear surface of the sphere and significant reduction in the form drag. However, this suction increased the friction drag. The blowing part did not much modify the surface pressure but decreased the skin friction. With this combined effect, the total drag was decreased significantly by the present suboptimal control. The lift coefficient also became zero or decreased significantly. The vortical structures in the wake were considerably modified due to the control. Finally, as the Reynolds number increased (within the range of Reynolds numbers considered), the amount of drag reduction increased and the control efficiency increased.

In the present study, an open-loop actuation profile was constructed for drag reduction from the results of suboptimal feedback control and produced good performance in drag reduction. Currently we are devising an 'optimal' open-loop actuation profile whose component consists of a few different wavelengths in the polar angle. We are also considering an active open-loop control where the blowing and suction are applied only on the limited area of the sphere surface. These results will be reported elsewhere.

Acknowledgement

This work was supported by the NRL Program (2009-0066334), KRF Grant (KRF-2007-412-J03001) and WCU Program of the Ministry of Education, Science, and Technology, Korea. Also, the authors would like to acknowledge the support from KISTI under "The Eighth Strategic Supercomputing Support Program".

References

Achenbach, E., 1974a. The effects of surface roughness and tunnel blockage on the flow past spheres. J. Fluid Mech. 65 (1), 113–125.
Achenbach, E., 1974b. Vortex shedding from spheres. J. Fluid Mech. 62, 209–221.
Anderson, E.A., Szewczyk, A.A., 1997. Effects of a splitter plate on the near wake of a circular cylinder in 2 and 3-dimensional flow configurations. Exp. Fluids 23 (2), 161–174.
Bagchi, P., 2007. Flow past a sphere with surface blowing and suction. J. Fluids Eng. 129, 1547.
Bearman, P.W., 1967. The effect of base bleed on the flow behind a two-dimensional model with a blunt trailing edge. Aeronaut. Quart., 207–224.
Bearman, P.W., Harvey, J.K., 1976. Golf ball aerodynamics. Aeronaut. Quart., 112–122.
Bearman, P.W., Owen, J.C., 1998. Reduction of bluff-body drag and suppression of vortex shedding by the introduction of wavy separation lines. J. Fluids Struct. 12 (1), 123–130.
Berger, E., 1967. Suppression of vortex shedding and turbulence behind oscillating cylinders. Phys. Fluids 10, S191.
Bergmann, M., Cordier, L., Brancher, J.P., 2005. Optimal rotary control of the cylinder wake using proper orthogonal decomposition reduced-order model. Phys. Fluids 17, 097101.
Bewley, T.R., 2001. Flow control: new challenges for a new Renaissance. Prog. Aerospace Sci. 37 (1), 21–58.
Choi, B., Choi, H., 2000. Drag reduction with a sliding wall in flow over a circular cylinder. AIAA J. 38 (4), 715–717.
Choi, H., Temam, R., Moin, P., Kim, J., 1993. Feedback control for unsteady flow and its application to the stochastic Burgers equation. J. Fluid Mech. 253, 509–543.
Choi, J., Jeon, W.-P., Choi, H., 2006. Mechanism of drag reduction by dimples on a sphere. Phys. Fluids 18, 041702.
Choi, H., Jeon, W.-P., Kim, J., 2008. Control of flow over a bluff body. Annu. Rev. Fluid Mech. 40, 113–139.
Collis, S.S., Joslin, R.D., Seifert, A., Theofilis, V., 2004. Issues in active flow control: theory, control, simulation, and experiment. Prog. Aerospace Sci. 40, 237–289.
Constantinescu, G., Squires, K., 2004. Numerical investigations of flow over a sphere in the subcritical and supercritical regimes. Phys. Fluids 16, 1449.
Cortelezzi, L., 1996. Nonlinear feedback control of the wake past a plate with a suction point on the downstream wall. J. Fluid Mech. 327, 303–324.
Cortelezzi, L., Chen, Y.C., Chang, H.L., 1997. Nonlinear feedback control of the wake past a plate: From a low-order model to a higher-order model. Phys. Fluids 9, 2009.
Darekar, R.M., Sherwin, S.J., 2001. Flow past a square-section cylinder with a wavy stagnation face. J. Fluid Mech. 426, 263–295.
Ffowcs, J.E., Zhao, B.C., 1989. The active control of vortex shedding. J. Fluids Struct. 3.
Fujisawa, N., Takeda, G., Ike, N., 2004. Phase-averaged characteristics of flow around a circular cylinder under acoustic excitation control. J. Fluids Struct. 19 (2), 159–170.
Fukagata, K., Sugiyama, K., Kasagi, N., 2009. On the lower bound of net driving power in controlled duct flows. Physica D 238 (13), 1082–1086.
Ghattas, O., Bark, J.H., 1997. Optimal control of two-and three-dimensional incompressible Navier–Stokes flows. J. Comput. Phys. 136 (2), 231–244.
Gillies, E.A., 1998. Low-dimensional control of the circular cylinder wake. J. Fluid Mech. 371, 157–178.
Graham, W.R., Peraire, J., Tang, K.Y., 1999. Optimal control of vortex shedding using low-order models. Part II: model-based control. Int. J. Numer. Methods Eng. 44, 973–990.
He, J.W., Glowinski, R., Metcalfe, R., Nordlander, A., Periaux, J., 2000. Active control and drag optimization for flow past a circular cylinder. 1: oscillatory cylinder rotation. J. Comput. Phys. 163 (1), 83–117.
Higuchi, H., 2005. Passive and active controls of three-dimensional wake of bluff-body. JSME Int. J. Ser. B 48 (2), 322–327.
Homescu, C., Navon, I.M., Li, Z., 2002. Suppression of vortex shedding for flow around a circular cylinder using optimal control. Int. J. Numer. Methods Fluids 38, 43–69.
Huang, X.Y., 1996. Feedback control of vortex shedding from a circular cylinder. Exp. Fluids 20 (3), 218–224.
Hwang, J.Y., Yang, K.S., Sun, S.H., 2003. Reduction of flow-induced forces on a circular cylinder using a detached splitter plate. Phys. Fluids 15, 2433–2436.
Jeon, S., Choi, H., 2009. Boundary treatment for unsteady surface velocity in an immersed boundary method. J. Mech. Sci. Technol. 23, 2502–2506.
Jeon, S., Choi, J., Jeon, W.-P., Choi, H., Park, J., 2004. Active control of flow over a sphere for drag reduction at a subcritical Reynolds number. J. Fluid Mech. 517, 113–129.
Jeong, J., Hussain, F., 1995. On the identification of a vortex. J. Fluid Mech. 285, 69–94.
Johnson, T.A., Patel, V.C., 1999. Flow past a sphere up to a Reynolds number of 300. J. Fluid Mech. 378, 19–70.
Kang, S., Choi, H., 2002. Suboptimal feedback control of turbulent flow over a backward-facing step. J. Fluid Mech. 463, 201–227.
Kim, J., Bewley, T.R., 2007. A linear systems approach to flow control. Annu. Rev. Fluid Mech. 39, 383.
Kim, D., Choi, H., 2002. Laminar flow past a sphere rotating in the streamwise direction. J. Fluid Mech. 461, 365–386.
Kim, J., Choi, H., 2005. Distributed forcing of flow over a circular cylinder. Phys. Fluids 17, 033103.
Kim, H.J., Durbin, P.A., 1988. Observations of the frequencies in a sphere wake and of drag increase by acoustic excitation. Phys. Fluids 31, 3260–3265.
Kim, J., Kim, D., Choi, H., 2001. An immersed-boundary finite volume method for simulations of flow in complex geometries. J. Comput. Phys. 171, 132–150.
Kim, J., Hahn, S., Kim, J., Lee, D., Choi, J., Jeon, W.-P., Choi, H., 2004. Active control of turbulent flow over a model vehicle for drag reduction. J. Turbul. 5, 019.
Kwon, K., Choi, H., 1996. Control of laminar vortex shedding behind a circular cylinder using splitter plates. Phys. Fluids 8, 479.
Lee, C., Kim, J., Choi, H., 1998. Suboptimal control of turbulent channel flow for drag reduction. J. Fluid Mech. 358, 245–258.
Li, F., Aubry, N., 2003. Feedback control of a flow past a cylinder via transverse motion. Phys. Fluids 15, 2163.
Li, Z., Navon, I.M., Hussaini, M.Y., Le Dimet, F.X., 2003. Optimal control of cylinder wakes via suction and blowing. Comput. Fluids 32 (2), 149–171.
Lin, J.C., Towfighi, J., Rockwell, D., 1995. Near-wake of a circular cylinder: control, by steady and unsteady surface injection. J. Fluids Struct. 9 (6), 659–669.
Milano, M., Koumoutsakos, P., 2002. A clustering genetic algorithm for cylinder drag optimization. J. Comput. Phys. 175 (1), 79–107.
Min, C., Choi, H., 1999. Suboptimal feedback control of vortex shedding at low Reynolds numbers. J. Fluid Mech. 401, 123–156.
Mittal, R., 1999. Planar symmetry in the unsteady wake of a sphere. AIAA J. 37, 388–390.
Mittal, R., Najjar, F.M., 1999. Vortex dynamics in the sphere wake. AIAA Paper, pp. 99–3806.
Niazmand, H., Renksizbulut, M., 2005. Flow past a spinning sphere with surface blowing and heat transfer. J. Fluids Eng. 127, 163.
Owen, J.C., Szewczyk, A.A., Bearman, P.W., 2000. Suppression of Karman vortex shedding. Phys. Fluids 12, 1–13.
Owen, J.C., Bearman, P.W., Szewczyk, A.A., 2001. Passive control of VIV with drag reduction. J. Fluids Struct. 15 (3–4), 597–605.
Ozono, S., 1999. Flow control of vortex shedding by a short splitter plate asymmetrically arranged downstream of a cylinder. Phys. Fluids 11, 2928.
Park, D.S., Ladd, D.M., Hendricks, E.W., 1994. Feedback control of von Karman vortex shedding behind a circular cylinder at low Reynolds numbers. Phys. Fluids 6, 2390.
Park, H., Lee, D., Jeon, W.-P., Hahn, S., Kim, J., Kim, J., Choi, J., Choi, H., 2006. Drag reduction in flow over a two-dimensional bluff body with a blunt trailing edge using a new passive device. J. Fluid Mech. 563, 389–414.
Petrusma, M.S., Gai, S.L., 1994. The effect of geometry on the base pressure recovery of segmented blunt trailing edges. Aeronaut. J. 98 (977), 267–274.
Poncet, P., Koumoutsakos, P., 2005. Optimization of vortex shedding in 3-D wakes using belt actuators. Int. J. Offshore Polar Eng. 15 (1), 7–13.
Poncet, P., Hildebrand, R., Cottet, G.H., Koumoutsakos, P., 2008. Spatially distributed control for optimal drag reduction of the flow past a circular cylinder. J. Fluid Mech. 599, 111–120.
Protas, B., 2004. Linear feedback stabilization of laminar vortex shedding based on a point vortex model. Phys. Fluids 16, 4473.
Protas, B., Styczek, A., 2002. Optimal rotary control of the cylinder wake in the laminar regime. Phys. Fluids 14, 2073.
Rodriguez, O., 1991. Base drag reduction by control of the three-dimensional unsteady vortical structures. Exp. Fluids 11 (4), 218–226.
Roussopoulos, K., 1993. Feedback control of vortex shedding at low Reynolds numbers. J. Fluid Mech. 248, 267–296.
Sakamoto, H., Haniu, H., 1990. A study on vortex shedding from spheres in a uniform flow. Trans. ASME: J. Fluids Eng. 112, 386–392.
Shih, W.C.L., Wang, C., Coles, D., Roshko, A., 1994. Experiments on flow past rough circular cylinders at large Reynolds numbers. J. Wind Eng. Ind. Aerodyn. 49 (1), 351–368.
Suryanarayana, G.K., Meier, G.E.A., 1995. Effect of ventilation on the flowfield around a sphere. Exps. Fluids 19, 78–88.
Taneda, S., 1978. Visual observations of the flow past a sphere at Reynolds numbers between 10^4 and 10^6. J. Fluid Mech. 85 (1), 187–192.

Tanner, M., 1972. A method of reducing the base drag of wings with blunt trailing edges. Aeronaut. Quart. 23, 15–23.
Tombazis, N., Bearman, P.W., 1997. A study of three-dimensional aspects of vortex shedding from a bluff body with a mild geometric disturbance. J. Fluid Mech. 330, 85–112.
Williams, D.R., Mansy, H., Amato, C., 1992. The response and symmetry properties of a cylinder wake subjected to localized surface excitation. J. Fluid Mech. 234, 71–96.
Wood, C.J., 1964. The effect of base bleed on a periodic wake. J.R. Aeronaut. Soc. 68, 477.
Yun, G., Kim, D., Choi, H., 2006. Vortical structures behind a sphere at subcritical Reynolds numbers. Phys. Fluids 18, 015102.
Zdravkovich, M.M., 1981. Review and classification of various aerodynamic and hydrodynamic means for suppressing vortex shedding. J. Wind Eng. Ind. Aerodyn. 7 (2), 145–189.